

Glucose Sensing Optionally in Optical and Optoelectrical Modes Based on Au-TiO₂ Schottky Nanojunctions

Lu Ma, Weijian Zhu, Linling Qin, Donglin Pu*, and Shaolong Wu*

School of Optoelectronic Science and Engineering & Key Lab of Advanced Optical Manufacturing Technologies of Jiangsu Province, Soochow University, Suzhou 215006, China

Abstracts: In recent years, metallic nanostructures have been extensively researched in the field of plasmonic for optical and optoelectronic applications such as biochemical sensing. However, an additional optoelectronic converter or spectrometer is usually required for the sensing application. Herein, the orderly-patterned Au-TiO₂ Schottky junction with an Al film that we coupled, which simultaneously works as an optical reflector and conducting layer, can achieve optical sensing of glucose by exciting surface plasmon resonance associated with the environment, and meanwhile can realize glucose detection with direct electrical-signal readout by collecting the photogenerated carriers inside the Au nanostructures and TiO₂ film. When used in optical mode, the designed sensor shows a sensing sensitivity of up to 1200.0 nmRIU⁻¹ in numerical calculation, and the measured value is 346.1 nmRIU⁻¹. When used in optoelectrical mode, the glucose sensor under one-sun illumination obtains a sensitivity of 70.0 μAM⁻¹cm⁻² in the concentration range of 0–10 mM, with a detection limit of 0.05 μM (Signal/Noise=3). Simulation and experimental results demonstrated that the Al-film-coupled Au-TiO₂ Schottky nanojunction can monitor glucose concentration optionally in optical and optoelectrical modes, which presents an alternative route to the miniaturized, portable, and multi-functioned sensors.

Keywords: Plasmonics, Glucose detection, Optical sensor, Photoelectrochemical cell, Au nanoholes, Schottky junction.

1. INTRODUCTION

Diabetes mellitus, a metabolic disease characterized by persistent higher-than-normal blood glucose values, causes chronic damage to various tissues, and dysfunction. According to a report on disease statistics released by the International Diabetes Federation (IDF), the prevalence of diabetes is growing at an alarming rate worldwide and is expected to reach 592 million people by 2035. Real-time monitoring of human blood glucose can effectively prevent abnormal blood glucose concentration. Currently, most of the human glucose meters on the market are based on electrochemical sensors. The electrochemical sensor relies on an electrode with glucose oxidase to contact the blood for a redox reaction [1, 2], and an ammeter detects the bioelectric current in the reaction and processes it to calculate the current glucose content in the blood, which can satisfy the need for certain portability. However, it usually requires the assistance of glucose enzymes and the addition of a bias voltage, which results in the electrochemical glucose sensor being vulnerable to the effects of environmental conditions, such as temperature, pH, etc. The homologous origin of the excitation signal of the electrochemical sensor from the

detected signal also leads to the background noise, which results in the detection limit being too high or insufficient anti-interference ability.

Besides the electrochemical sensors, optical glucose sensors are also attracting attention due to their long service life and short testing time. Among them, optical glucose sensors are mostly based on surface plasmon resonance (SPR). Plasma, an emerging interdisciplinary field, has received extensive attention in recent years due to the unique optical properties of these metallic microstructures and nanostructures. Since the discovery of extraordinary optical transmission (EOT) by Ebbesen [3] and others, subwavelength nanohole-perforated metal films have been a hot research topic in the field of plasmonics. Subsequently, metal nanohole array structures have been used in various applications, including optical filters [4], photovoltaic devices [5], enhanced fluorescence spectroscopy [6] and Raman scattering spectroscopy [7], DNA/RNA sequencing [8], seawater desalination [9], etc. Among them, the sensing application [10] has been a hot topic in recent years.

The structure of metal nanohole arrays (NHAs) can excite two modes of surface plasmon, *i.e.*, surface plasmon polariton (SPP) [11] and local surface plasmon (LSP) [12]. The SPP propagates along the metal-dielectric interface and is bound to the surface. This property makes it highly sensitive to changes in the refractive index environment close to the metal

*Address correspondence to this author at the School of Optoelectronic Science and Engineering & Key Lab of Advanced Optical Manufacturing Technologies of Jiangsu Province, Soochow University, Suzhou 215006, China; E-mail: pudonglin@suda.edu.cn; shaolong_wu@suda.edu.cn

surface. In the specific case of NHAs, the localized surface plasmon resonance (LSPR) property is present in the edge portion of the holes. The refractive-index sensitivity can be increased by modulating their period and diameter [13]. NHAs-based sensors can operate in normal incidence transmission mode [14] and can monitor analytes by observing variations in the transmission spectrum. This property helps in the design of devices that are easy to integrate into miniaturized ones, which is the main advantage of NHAs sensors. NHAs-based sensors have the advantages of real-time detection, high sensitivity, rapid testing, and no need for biomarkers. So far, sensors based on NHAs have been used for proteins [15], viruses [16, 17], bacteria [18], and so on. However, optical sensors usually require external photodetectors or spectrometers for testing, which are not suitable for non-professional implementation and in-situ inspection. For this reason, there is an urgent need for the optoelectrical sensors with a direct readout of the electrical signal.

Photoelectrochemical (PEC) analysis technology is a new sensing technology emerging in recent years, exuding fascinating potential with the advantages of low background noise, easy integration, high sensitivity, etc. PEC sensors successfully combine optical and electrochemical sensors by utilizing photoactive materials that absorb light. Through using light as the excitation source of the signal and an electrical signal as the signal output for detection, PEC sensors can achieve effective separation of the input signal and output signal, and avoid the shortcomings of high background noise of electrochemical sensors [19, 20]. However, the PEC sensors are usually insensitive to the light source. Therefore, developing a novel sensor with multifold working modes is of great significance when monitoring analytes with various concentrations, scenarios, and self-check function is required.

In this work, we first designed an optical sensor based on the nanoholed metal-semiconductor-metal structure by numerical simulation, and then successfully prepared the as-designed nanostructure. Experimental results show that by monitoring the central wavelength shift of the SPR and observing the photocurrent of the photoelectrode based on the nanoholed metal-semiconductor-metal structure under simulated solar illumination, glucose sensing with a large concentration range can be achieved via the same structure optionally in optical mode and optoelectrical mode. In addition, high sensitivity,

satisfactory selectivity, and good stability were obtained.

2. MATERIALS AND METHOD

2.1. Device Design and Numerical Simulation

Device design was performed via numerical simulation, e.g., using commercial software (FDTD Solutions). The finite element method was used to solve the electromagnetic field distribution of complex structures by differentially subdividing the complex geometry into a finite number of tiny cells. The approximate solutions for the optical absorption and the electromagnetic field distribution of the device structure could be calculated by introducing and varying the time variable into Maxwell's system of equations. The refractive index of TiO_2 materials was obtained from ellipsometry (Semilab, GES5E) tests for the as-prepared samples. The refractive index of the metallic materials was obtained by the Lorentz-Drude model. In the simulation, a reasonable simulation region and mesh accuracy were set according to the simulation requirements. In the device simulation region, the z-direction was the perfect matching layer (PML), which is an absorbing boundary condition that matches the impedance of the surrounding material, and the periodic boundary was used in the horizontal direction of x and y. A planar light was used, and the angle of incidence was 0° (along the -z direction).

2.2. Materials

SiO_2/Si substrate was purchased from Suzhou Yancai Technology Co. Ltd. Al targets and TiO_2 targets were purchased from Zhongnuo Advanced Materials (Beijing) Technology Co. Ltd. Dopamine (DA) was purchased from McLean Co. Ltd. Glucose, urea, lactic acid (LA), sodium chloride (NaCl), ascorbic acid (AA), and uric acid (UA) were purchased from Aladdin Co. Ltd. Ethanol, acetone, and sucrose were purchased from Shanghai Guoyao Co. Ltd. The water used in the experiment was deionized water with an electrical resistivity of $>18.25 \text{ M}\Omega\cdot\text{cm}$. Phosphate buffer solution (PBS) was purchased from Phygene Co. Ltd. All the chemical reagents were of analytical grade and did not require further purification.

2.3. Device Preparation and Characterization

The SiO_2/Si substrate was firstly ultrasonically cleaned by acetone, ethanol, and deionized water in turn. Next, a 100 nm-thick film of Al was sputtered on the cleaned substrate through DC magnetron

sputtering (LN-1082FS, Shenyang Lining Vacuum Technology Research Institute). Then, a 150 nm-thick film of TiO_2 was sputtered on the prepared substrate mentioned above through RF magnetron sputtering. The substrates covered by TiO_2/Al films were heated in air at 500 °C for 2 hours. Afterward, ordered photoresist nanopatterns were prepared on the above-prepared samples using laser direct writing (Miscan200, SVG Tech Group. Ltd). After the completion of the laser direct writing step, the sample was put into the developer to wash away the unnecessary photoresist. Then Au with a nominal thickness of 40 nm was evaporated on the patterned photoresist by using electron beam evaporation (Ei-5z, ULVAC). The obtained sample was immersed in acetone solution for 3 hours to complete lift-off. Finally, Au NHAs/ TiO_2/Al structure was obtained.

The device morphology was characterized by using a hot field emission scanning electron microscopy (SEM) (ZEISS, Sigma 300). Optical spectra and sensing tests were performed using a fiber optic spectrometer (NIRUE512, Ocean Optics) and an FTIR spectrometer (Nicolet iS50 FTIR, Thermo Fisher). The refractive index of analyte was changed by configuring glucose with different concentrations in deionized water, and its refractive index was tested by using an Abbe refractometer (WAY-2S, Shanghai Zhenghong Industrial). Unless otherwise specified, we investigated PEC behavior and sensing performance by using an electrochemical workstation (Zennium, Zahner CIMPS) in a three-electrode configuration under simulated AM 1.5G solar illumination (Enlitech, SS-F7-3A), whose intensity was calibrated by a standard solar cell to 100 mWcm^{-2} . An Ag/AgCl electrode immersed in saturated KCl solution was used as the reference electrode; An electrode made of Pt mesh was utilized as the counter electrode, and the as-prepared Au NHAs/ TiO_2/Al structure was used as the working electrode. For PEC sensing, 0.1 M PBS was used as the background solution and placed in a quartz photolysis cell. Current versus potential curves were recorded at a scan rate of

10 mV/s in the range of - 0.1 V to 0.5 V (vs. Ag/AgCl). Glucose sensing tests were performed under AM 1.5G illumination at 0 V (vs. Ag/AgCl). The working electrode was placed into a configured background solution containing concentration-varying glucose firstly in the dark, and the loop of light on-off was 60s. Sensitivity, selectivity, and stability tests were also performed under these conditions.

3. RESULTS AND DISCUSSION

3.1. Device Structure

Schematic of the designed sensor is shown in Figure 1. Note that an insulating substrate is used and not shown. The device structure consists of a substrate, Al film, TiO_2 film, and Au NHAs. As mentioned before, the Au NHAs can effectively regulate and reinforce the local electric field. The Al film can form a resonant cavity with the Au NHAs, meanwhile, the Al film will block the transmission of light from the resonant cavity. And the TiO_2 film acts as a spacer in optical sensing and photoelectrically active material in optoelectrical sensing. The geometrical parameters of the designed sensor are shown in Table 1, where h_1 denotes the thickness of the TiO_2 layer, h_2 denotes the thickness of the Au nanohole, P denotes the period of the Au gold nanoholes (*i.e.*, the distance between two neighboring nanoholes in the tetragonally aligned array), and r denotes the radius of the Au nanohole. The schematic flow diagram of the preparation process of the Au NHAs/ TiO_2/Al structure is shown in Figure 2(a). Figure 2(b-d) shows the top-view SEM images of the Au NHAs/ TiO_2/Al structure during the experimental preparation. Figure 2(b) shows the counter-structure of the NHAs obtained by using the laser direct writing technique. One can see that the as-deposited TiO_2/Al films are not perfectly smooth, and the sidewalls of the photoresist nanorods are not steep and straight, but with an angle to the vertical direction. After the evaporated deposition of Au in Figure 2(c), it can be seen that the grainy surface of

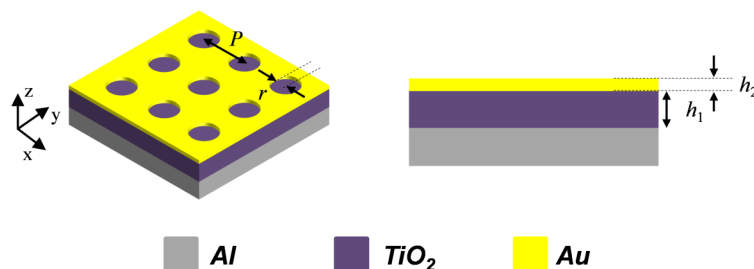


Figure 1: Schematic structure of the proposed sensor.

the structure is pronounced due to the unevenness of the prepared TiO_2/Al films, and it can also be seen more clearly that the sidewalls of the residual photoresist are not steep and straight. Figure 2(d) is the SEM image of the sample in Figure 2(c) after performing the stripping process to remove the remaining photoresist. The diameters of these nanoholes were measured to be 800 ± 50 nm. Note that the sample was immersed in an acetone solution and ultrasonically treated to perform the lift-off, which produces slight damage to the gold film and leads to the shapes of the as-obtained nanoholes being distorted.

Table 1: Geometrical Parameters of the Proposed Sensor

Parameter	Symbol	Quantity	Unit
Height of the TiO_2 layer	h_1	150	nm
Height of the Au layer	h_2	40	nm
Period of Au NHAs	P	1300	nm
The radius of Au NHs	r	400	nm

3.2. Optical Properties and Optical Sensing

The spectral characteristics of the designed structure are calculated and shown in Figure 3. Compared with the case in air, the characteristic reflection dips of the background solution changing to water show an obvious red shift, indicating a high refractive index sensitivity. When the background medium is water, there are three characteristic reflection valleys in the wavelength range of interest, with the central wavelengths respectively at 1286 nm, 1810 nm, and 2245 nm. To describe it conveniently, these reflection valleys are labeled as dip 1, dip 2, and dip 3 in sequence. To uncover the intrinsic reasons for the generation of the above characteristic dips, we carried out spatial monitoring and analysis of the magnetic field, as shown in Figure 4. To make the contrast of magnetic field between these three reflection valleys more obvious, the magnetic field planar (x-y plane at Au- TiO_2 interface) profiles map of dip 1, which has a weaker magnetic field strength, is selected for normalization, and other magnetic field maps are normalized relative to that of dip 1. In the

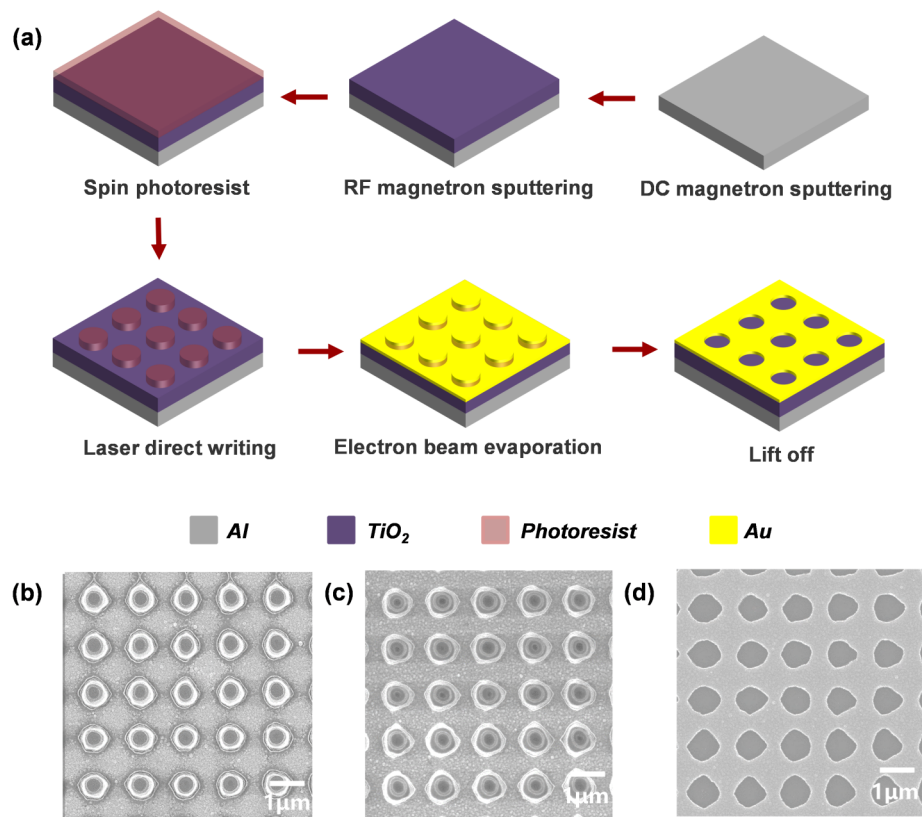


Figure 2: (a) Flowchart of the preparation process of the Au NHAs/ TiO_2 /Al structure. (b) Top-view SEM image of the photoresist nanorods. (c) Top-view SEM image of the photoresist nanorods covered with Au film. (d) Top-view SEM image of the obtained Au NHAs/ TiO_2 /Al structure.

case of dip 1, the magnetic field is mainly concentrated on the upper surface of the Al layer and partly on the upper surface of the Au NHAs. This indicates that the hybridized SPPs at the Au-water and Al-TiO₂ interfaces are excited; In the case of dip 2, the magnetic field is concentrated above the Al layer and at the edges of the Au NHAs due to the SPR effect at the Al-TiO₂ interface and the LSPR properties at the edge of the holes; In the case of dip 3, it can be seen that the magnetic field is strongly concentrated in the gap between the Au NHAs and the Al layer, which is due to the excitation of the SPR [21] at the Al-TiO₂ interface and the fact that the Al layer acts as a metallic reflector, which will block the transmission of the light from the resonance cavity, and the together lead to the enhancement of the magnetic field. As can be seen from the longitudinal profile of dip 3, the magnetic field is mainly localized between Au NHAs and Al, and the magnetic field strength at the surface is weak, thus providing limited sensitivity to changes in the surface refractive index, and being not suitable for refractive index sensing. While dip 1 and dip 2 have a strong magnetic field distribution on the top surface of the structure, therefore dip 1 and dip 2 are more suitable for refractive index sensing.

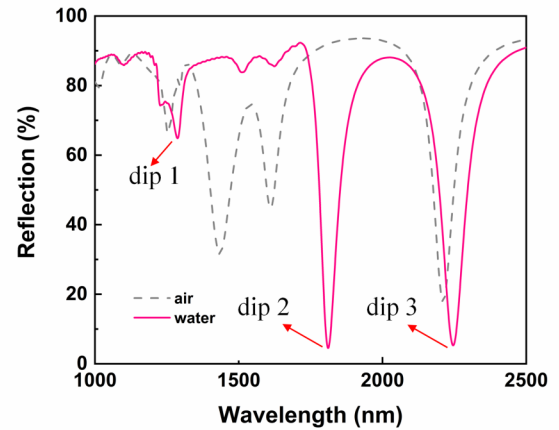


Figure 3: Calculated reflection spectra of the designed sensor.

To determine the sensitivity of the structure as a refractive index sensor, we configured different concentrations of glucose aqueous solutions for sensitivity testing. The concentrations of the configured glucose aqueous solutions were 0 M, 1 M, 2 M, 3 M, and 4 M, and the measured refractive index were 1.3333, 1.3561, 1.3712, 1.3891, and 1.4006 in sequence. Figure 5(a) shows the simulated spectra with the background refractive index increasing from 1.33 to 1.43, and dip 1 shows an obvious redshift, which can be attributed to the excitation of the SPR at

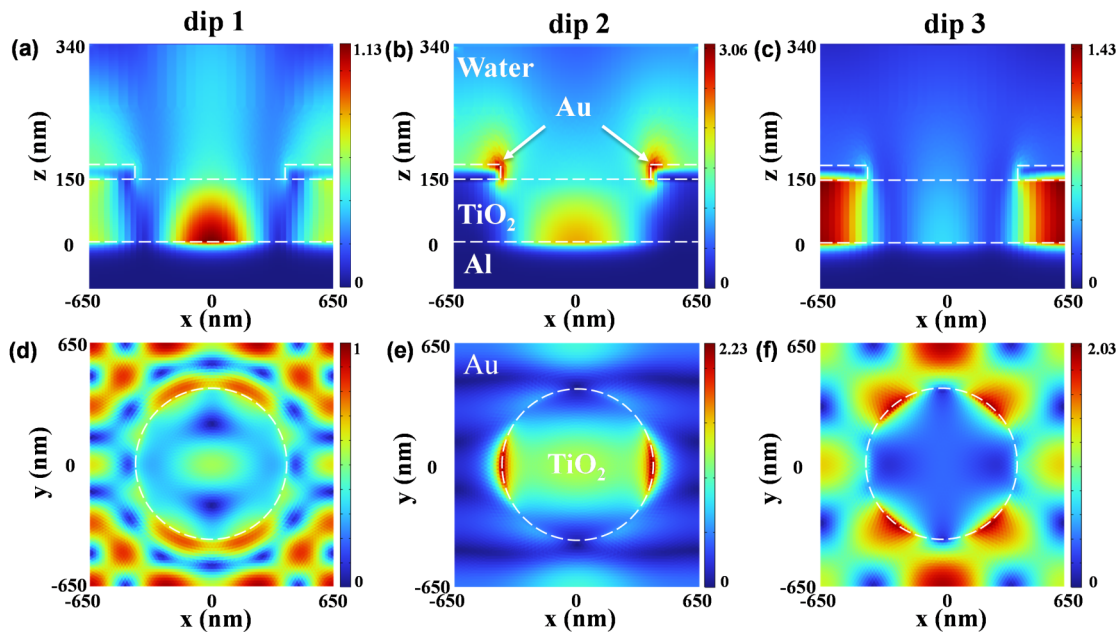


Figure 4: Spatial distribution of the normalized magnetic field of the designed sensor in water. (a) and (d) are the longitudinal (x-z plane) and planar (x-y plane at Au-TiO₂ interface) profiles of the normalized magnetic field distribution at the wavelength of 1286 nm (dip 1); (b) and (e) are the longitudinal (x-z plane) and planar (x-y plane at Au-TiO₂ interface) profiles of the normalized magnetic field distribution at the wavelength of 1810 nm (dip 2); (c) and (f) are the longitudinal (x-z plane) and planar (x-y plane at Au-TiO₂ interface) profiles of the normalized magnetic field distribution at the wavelength of 2245 nm (dip 3).

the Au-water interface, resulting in the surface being sensitive to the change in refractive index. Figure 5(b) is the experimentally measured data, and the spectrum redshift is consistent with the simulation results. Figure 5(c) plots the linear fits of the resonance wavelength of dip 1 as a function of the refractive index of the surrounding medium in simulation and experiment, and the slope is the sensitivity. In our experiments, based on the concentration (C) of the configured solution and its measured refractive index (n), we obtained an empirical formula, *i.e.*, $n = 0.017C + 1.3333$. The calculated sensitivity is 448.9 nmRIU^{-1} , and the corresponding measured sensitivity is 252.5 nmRIU^{-1} , converting to a concentration sensitivity of 14853.0 nmM^{-1} for the observed resonance wavelength. Figure 5(d-f) shows the simulation, experiment, and sensitivity fitting of the spectra around dip 2. The fitted sensitivity is $1200.0 \text{ nmRIU}^{-1}$ in the simulation and 346.1 nmRIU^{-1} (converting to a concentration sensitivity of 20356.5 nmM^{-1}) in the experiment. By researching the spectral response of the structure to different background refractive index, it is shown that the structure can be used for high-sensitivity sensing of experimental refractive index. One may also note that there are significant differences in the fitting sensitivities and the

central wavelengths corresponding to the same resonances between the simulation and experiment due to the following two factors: (1) the periodic nanostructure designed in the simulation is perfect and without defects, but there are unavoidable defects in the shape, period, and surface roughness for the experiment preparation; (2) the real thickness and evenness of each material layer prepared by experiments cannot be perfectly matched comparing with the design.

3.3. Photoelectrochemical Behaviors and Optoelectronic Sensing

For the optoelectronic sensing, the Al film plays the role of reflector and back electrode, TiO_2 film is the photoelectrically active material, and the coupling of Au NHAs and TiO_2 film can form a Schottky barrier, which can improve the photocurrent response. As mentioned previously, with LSPR properties at the edge part of the hole, under simulated sunlight, Au NHAs absorb light to produce hot electron-hole pair (Eq. 1), the generated hot electrons can pass through the Schottky junction formed by the Au NHAs and reach the conduction band of the TiO_2 film [22]. The TiO_2 also absorbs the UV light

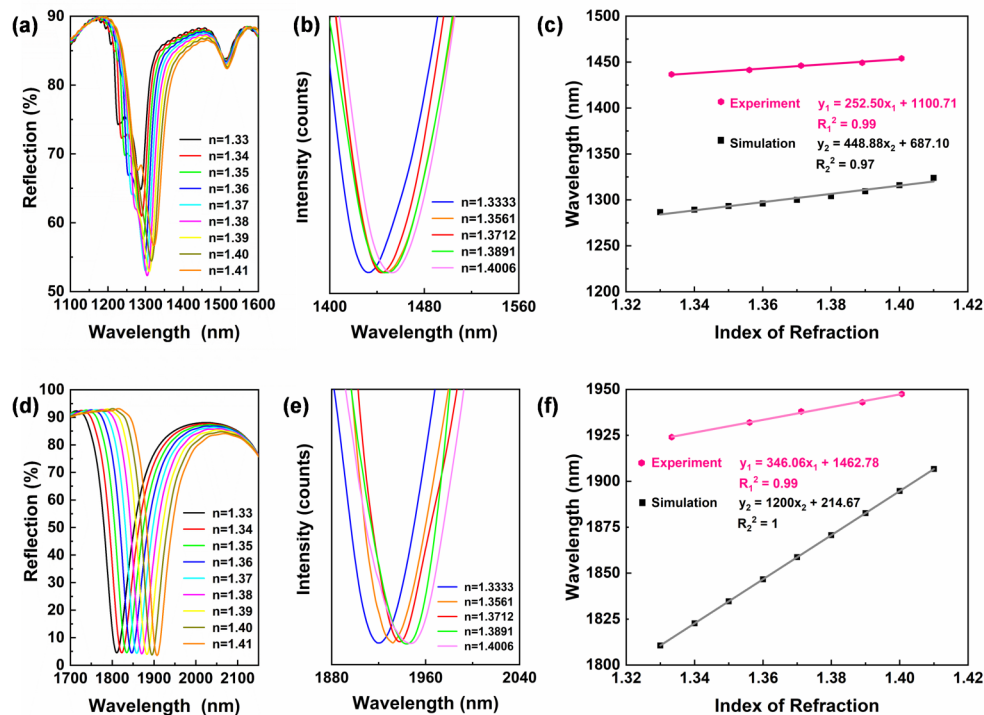


Figure 5: (a) Simulated and (b) experimental reflection spectra around dip 1 at different backgrounds with different refractive index, and (c) a linear fit of the simulated and experimental resonance wavelengths as a function of the refractive index of the background. (d) Simulated and (e) experimental reflection spectra around the dip 2 at different backgrounds with different refractive index, and (f) a linear fit of the simulated and experimental resonance wavelengths as a function of the refractive index of the background.

[23] and generates the photogenerated electron-hole pairs (Eq. 2), and the electrons inside the TiO₂ are extracted to the counter electrode through the rear electrode [24], while the photogenerated holes react with glucose (*i.e.*, oxidizing glucose to gluconic acid) (Eq. 3). In the course of these several physical/chemical reactions, photogenerated carriers are sufficient, and the observed photocurrent is limited only by the glucose concentration. When the glucose concentration changes, the number of photogenerated holes on the sensing photoelectrode surface involved in glucose oxidation changes accordingly, so the current density increases with the increase of glucose concentration.

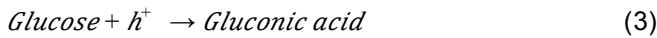


Figure 6 shows the current-potential (*J-V*) behavior of the Au NHAs/TiO₂/Al photoelectrode in the concentration-varying glucose. The black line shows the *J-V* plot of the device in the dark state, which shows that the device has a good rectification effect, implying the formation of Schottky junctions. This characteristic is beneficial to suppress the noise current of the sensor. Under light conditions, a gradual increase in photocurrent with increasing scanning potential and glucose concentration is clearly observed, which is attributed to the increase of the number of glucose molecules in solution as well as the increase of the applied bias pressure that favors the oxidation of glucose. Although the external bias voltage will increase the photocurrent, it will also lead to an increase of the dark current and will also damage the

electrodes. After comprehensive consideration, we choose 0 V (vs. Ag/AgCl) as the operation bias. Figure 7 exhibits the photoelectrochemical sensing performance of the Au NHAs/TiO₂/Al structure. As shown in Figure 7(a), when the light is off, there is only a background current of several nanoampere (nA). In contrast, once the AM 1.5G simulated sunlight is on, the current rapidly up to microampere (μA), and the photocurrent is directly proportional to the glucose concentration. Figure 7(b) is the fitting curve of the photocurrent with the glucose concentration, and it can be known that in the concentration range of 0–10 mM range, the fitting sensitivity is 70.0 μA⁻¹cm⁻², and the corresponding detection limit can be calculated to be 0.05 μM (Signal/Noise = 3). Considering that the normal blood glucose range of the human body is 3.9–6.1 mM, which is surrounded by the test range of our sensor, it confirms that our sensor can perform blood glucose detection.

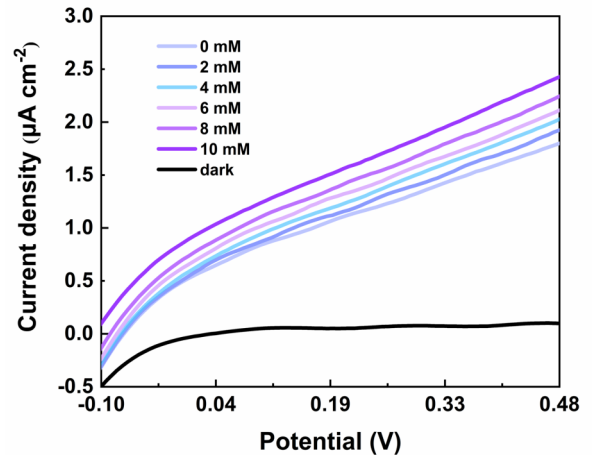


Figure 6: Current-potential behavior of the prepared Au NHAs/TiO₂/Al photoelectrodes in concentration-varying glucose solutions under one-sun illumination and in the dark.

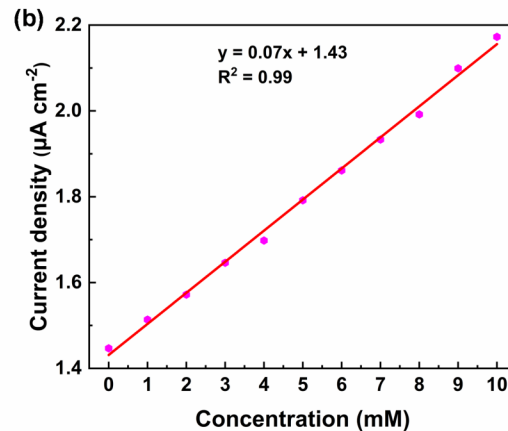
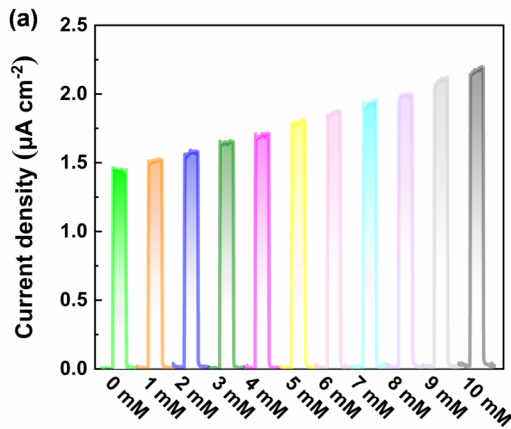


Figure 7: (a) Photocurrent responses of the prepared Au NHAs/TiO₂/Al photoelectrodes in concentration-varying glucose solutions at relatively zero bias. (b) Calibration curve versus glucose concentration. R²: regression coefficient.

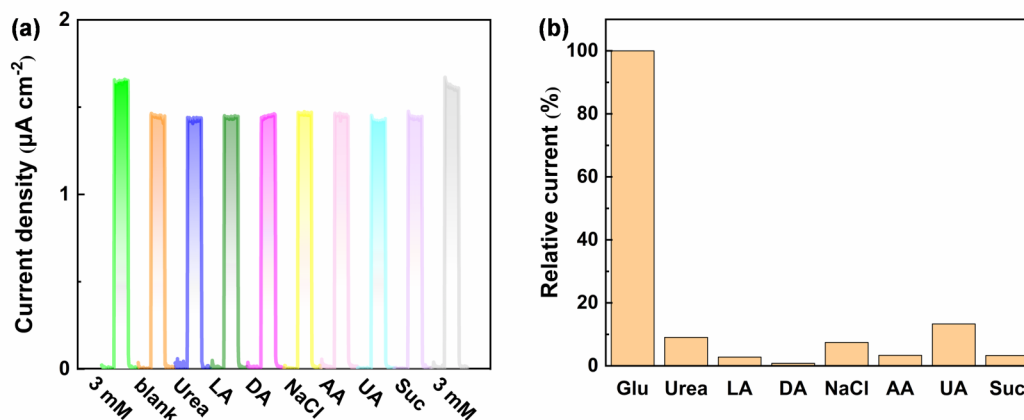


Figure 8: (a) Photocurrent response of the prepared Au NHAs/TiO₂/Al photoelectrodes at relatively zero bias with the addition of different substances (3 mM Glucose, 0.1 mM Urea, 0.1 mM LA, 0.01 mM DA, 145 mM NaCl, 0.1 mM Urea, 0.1 mM AA, 0.1 mM UA, 0.1 mM Suc) into background solution. (b) Statistical analysis of (a).

To illustrate the performance of the Au NHAs/TiO₂/Al structure for real glucose sensing, we further evaluated its selectivity, anti-interference, and stability. As shown in Figure 8(a), where we simulated the real situation in human body fluids by adding the substances coexisting with the body fluids [20], such as Urea, LA, DA, NaCl, UA, and Suc, as interfering substances to the background solution [25, 26]. It can be seen that when these interfering substances are added, the corresponding photocurrents are mildly different from that in the background solution, while there is a significant increase in the photocurrent when 3 mM glucose is added. As shown in Figure 8(b), after normalization using the photocurrent response of glucose as a benchmark, excepting for UA having some interference ($\sim 13\%$), the interference effects of Urea, LA, DA, NaCl, and Suc on the photocurrents are small ($< 10\%$), which do not produce an obvious change in photocurrent relative to the introduction of glucose. These results show that our prepared sensor based on the Au NHAs/TiO₂/Al structure has good selectivity for glucose detection.

Figure 9 shows the continuous photocurrent response under multiple switching of light at 1 min intervals over 30 min, and the result shows that the attenuation of the photocurrent density is within 10%. The current density of the PEC sensing photoelectrode decreases with operation time. This phenomenon can be ascribed to the glucose concentration in the solution (especially these regions close to the electrode surfaces) decreases with the increase of the test time, which is because the process of glucose oxidation to gluconic acid is irreversible. It indicates that our prepared sensor also has good stability. Moreover, since the sensor can produce photocurrent both from

the metal nanostructure and the photoactive semiconductor, it means that the widely-used compound light or sunlight can be used as a light source, without requiring a specific spectrometer or monochromatic light of a specific wavelength, and the glucose-sensing can be achieved with direct readout of electrical signal.

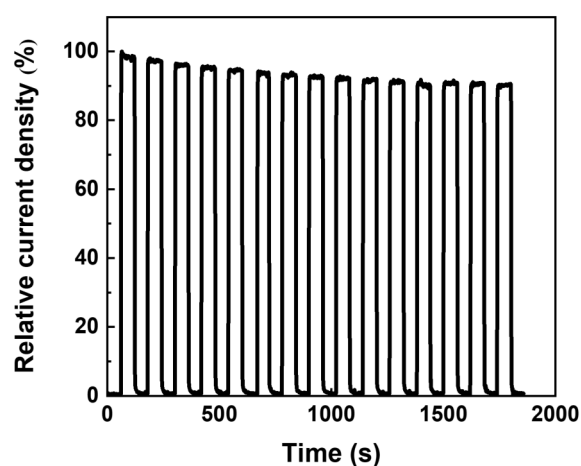


Figure 9: Current-time plot of the prepared Au NHAs/TiO₂/Al photoelectrodes switching the light on and off for 30 min operation in the background solution containing 3 mM glucose.

4. CONCLUSIONS

In this work, we present an optical and optoelectrical dual-mode glucose sensor based on Al-film-coupled Au-TiO₂ nanojunction. The optical sensing is mainly due to the SPR properties indicated by the Au NHAs and the Al layer blocking the transmission of light from the resonant cavity. We achieve the optical sensing function by monitoring its central wavelength

shift as changing the glucose concentration, with a sensitivity of $1200.0 \text{ nmRIU}^{-1}$ in numerical simulation, and the measured value is 346.1 nmRIU^{-1} . We also achieve glucose sensing by collecting the photocurrents from the interband absorption of TiO_2 film and intraband absorption of Au NHAs, with a sensitivity of $70.0 \mu\text{A M}^{-1}\text{cm}^{-2}$ under one-sun illumination. The direct electrical readout of sensing can be obtained with a common composite light or sunlight as the excitation source and without the need for a specific spectrometer or a monochromatic light of specific wavelength. Experiments further demonstrate that the sensor has good selectivity and stability. The demonstrated dual-mode sensor based on the Au NHAs/ TiO_2 /Al structure proposes a new platform for sensing glucose and also enriches the application of plasmonic devices.

ACKNOWLEDGMENTS

This research was financially supported by the National Natural Science Foundation of China (No. 62075146, and 62375192), Natural Science Foundation of Jiangsu Province (No. BK20231311), Qinglan Project of Jiangsu Province of China, and Priority Academic Program Development (PAPD) of Jiangsu Higher Education Institutions.

REFERENCES

- [1] Lipińska W, Siuzdak K, Karczewski J, *et al.* Electrochemical glucose sensor based on the glucose oxidase entrapped in chitosan immobilized onto laser-processed Au-Ti electrode. *Sens Actuators B Chem* 2021; 330: 129409. <https://doi.org/10.1016/j.snb.2020.129409>
- [2] Myndrul V, Coy E, Babayevska N, *et al.* MXene nanoflakes decorating ZnO tetrapods for enhanced performance of skin-attachable stretchable enzymatic electrochemical glucose sensor. *Biosens Bioelectron* 2022; 207: 114141. <https://doi.org/10.1016/j.bios.2022.114141>
- [3] Ebbesen TW, Lezec HJ, Ghaemi HF, *et al.* Extraordinary optical transmission through sub-wavelength hole arrays. *Nature* 1998; 391(6668): 667-669. <https://doi.org/10.1038/35570>
- [4] Chen Q, Cumming DRS. High transmission and low color cross-talk plasmonic color filters using triangular-lattice hole arrays in aluminum films. *Opt Express* 2010; 18(13): 14056. <https://doi.org/10.1364/OE.18.014056>
- [5] Ostfeld AE, Pacifici D. Plasmonic concentrators for enhanced light absorption in ultrathin film organic photovoltaics. *Appl Phys Lett* 2011; 98(11): 113112. <https://doi.org/10.1063/1.3567543>
- [6] Brolo AG, Kwok SC, Moffitt MG, *et al.* Enhanced fluorescence from arrays of nanoholes in a gold film. *J Am Chem Soc* 2005; 127(42): 14936-14941. <https://doi.org/10.1021/ja0548687>
- [7] Zhang M, Chen T, Liu Y, *et al.* Three-dimensional TiO_2 -Ag nanopore arrays for powerful photoinduced enhanced Raman spectroscopy (PIERS) and versatile detection of toxic organics. *ChemNanoMat* 2019; 5(1): 55-60. <https://doi.org/10.1002/cnma.201800389>
- [8] Kasianowicz JJ, Brandin E, Branton D, *et al.* Characterization of individual polynucleotide molecules using a membrane channel. *Proc Natl Acad Sci USA* 1996; 93(24): 13770-13773. <https://doi.org/10.1073/pnas.93.24.13770>
- [9] Surwade SP, Smirnov SN, Vlassiuk IV, *et al.* Water desalination using nanoporous single-layer graphene with tunable pore size. *Nat Nanotechnol* 2015; 10(5): 459-464. <https://doi.org/10.1038/nnano.2015.37>
- [10] Li L, Wu S, Li L, *et al.* Gap-mode excitation, manipulation, and refractive-index sensing application by gold nanocube arrays. *Nanoscale* 2019; 11(12): 5467-5473. <https://doi.org/10.1039/C8NR09073D>
- [11] Willets KA, Van Duyne RP. Localized surface plasmon resonance spectroscopy and sensing. *Annu Rev Phys Chem* 2007; 58(1): 267-297. <https://doi.org/10.1146/annurev.physchem.58.032806.104607>
- [12] Kelly KL, Coronado E, Zhao LL, *et al.* The optical properties of metal nanoparticles: the influence of size, shape, and dielectric environment. *J Phys Chem B* 2003; 107(3): 668-677. <https://doi.org/10.1021/jp026731y>
- [13] Garcia-Vidal FJ, Martin-Moreno L, Ebbesen TW, *et al.* Light passing through subwavelength apertures. *Rev Mod Phys* 2010; 82(1): 729-787. <https://doi.org/10.1103/RevModPhys.82.729>
- [14] Monteiro JP, Carneiro LB, Rahman MM, *et al.* Effect of periodicity on the performance of surface plasmon resonance sensors based on subwavelength nanohole arrays. *Sens Actuators B Chem* 2013; 178: 366-370. <https://doi.org/10.1016/j.snb.2012.12.090>
- [15] Yanik AA, Cetin AE, Huang M, *et al.* Seeing protein monolayers with naked eye through plasmonic Fano resonances. *Proc Natl Acad Sci* 2011; 108(29): 11784-11789. <https://doi.org/10.1073/pnas.1101910108>
- [16] Yanik AA, Huang M, Kamohara O, *et al.* An optofluidic nanoplasmonic biosensor for direct detection of live viruses from biological media. *Nano Lett* 2010; 10(12): 4962-4969. <https://doi.org/10.1021/nl103025u>
- [17] Jackman JA, Linardy E, Yoo D, *et al.* Plasmonic nanohole sensor for capturing single virus-like particles toward virucidal drug evaluation. *Small* 2016; 12(9): 1159-1166. <https://doi.org/10.1002/sml.201501914>
- [18] Gomez-Cruz J, Nair S, Manjarrez-Hernandez A, *et al.* Cost-effective flow-through nanohole array-based biosensing platform for the label-free detection of uropathogenic *E. coli* in real time. *Biosens Bioelectron* 2018; 106: 105-110. <https://doi.org/10.1016/j.bios.2018.01.055>
- [19] Ke S, Qin L, Zhang R, *et al.* Towards self-driven and enzyme-free sweat glucose photoelectrochemical sensing via decorating CuO nanoparticles on TiO_2 hierarchical nanotubes. *Surf Interfaces* 2023; 40: 103102. <https://doi.org/10.1016/j.surfin.2023.103102>
- [20] Zhang R, Ke S, Lu W, *et al.* Constructing a Si-CuO core-shell nanowire heterojunction photoanode for enzyme-free and highly-sensitive glucose sensing. *Appl Surf Sci* 2023; 632: 157593. <https://doi.org/10.1016/j.apsusc.2023.157593>
- [21] Tang H, Chen CJ, Huang Z, *et al.* Plasmonic hot electrons for sensing, photodetection, and solar energy applications: A perspective. *J Chem Phys* 2020; 152(22): 220901. <https://doi.org/10.1063/5.0005334>
- [22] Saha S, Victorious A, Soleymani L. Modulating the photoelectrochemical response of titanium dioxide (TiO_2) photoelectrodes using gold (Au) nanoparticles excited at different wavelengths. *Electrochim Acta* 2021; 380: 138154. <https://doi.org/10.1016/j.electacta.2021.138154>

- [23] Esmaeili FO, Tasviri M, Mohaghegh N. A Cd_x Zn_{1-x} S/TiO₂ nanotube array electrode for a highly sensitive and selective nonenzymatic photoelectrochemical glucose sensor. *New J Chem* 2022; 46(20): 9880-9888. <https://doi.org/10.1039/D2NJ00549B>
- [24] Yu Y, Qin L, Lu W, *et al.* Unbiased glucose biosensing based on Al film coupled TiO₂ film/Au nanoparticles Schottky junction toward low concentration and wide range detection. *ACS Appl Nano Mater* 2022; 5(8): 11776-11786. <https://doi.org/10.1021/acsnm.2c02770>
- [25] Li YL, Tian J, Shi DJ, *et al.* CdSe/TiO₂NTs heterojunction-based nonenzymatic photoelectrochemical sensor for glucose detection. *Langmuir* 2023; 39(42): 14935-14944. <https://doi.org/10.1021/acs.langmuir.3c01685>
- [26] Li M, Wang H, Wang X, *et al.* Ti₃C₂/Cu₂O heterostructure based signal-off photoelectrochemical sensor for high sensitivity detection of glucose. *Biosens Bioelectron* 2019; 142: 111535. <https://doi.org/10.1016/j.bios.2019.111535>

Received on 20-01-2024

Accepted on 21-02-2024

Published on 27-02-2024

DOI: <https://doi.org/10.31875/2410-2199.2024.11.01>© 2024 Ma *et al.*; Zeal Press.

This is an open access article licensed under the terms of the Creative Commons Attribution License

[\(http://creativecommons.org/licenses/by/4.0/\)](http://creativecommons.org/licenses/by/4.0/) which permits unrestricted use, distribution and reproduction in any medium, provided the work is properly cited.